REVIEW

Protein structural dynamics revealed by site-directed spin labeling and multifrequency EPR

Yuri E. Nesmelov · David D. Thomas

Abstract Multifrequency electron paramagnetic resonance (EPR), combined with site-directed spin labeling, is a powerful spectroscopic tool to characterize protein dynamics. The lineshape of an EPR spectrum reflects combined rotational dynamics of the spin probe's local motion within a protein, reorientations of protein domains, and overall protein tumbling. All these motions can be restricted and anisotropic, and separation of these motions is important for thorough characterization of protein dynamics. Multifrequency EPR distinguishes between different motions of a spin-labeled protein, due to the frequency dependence of EPR resolution to fast and slow motion of a spin probe. This gives multifrequency EPR its unique capability to characterize protein dynamics in great detail. In this review, we analyze what makes multifrequency EPR sensitive to different rates of spin probe motion and discuss several examples of its usage to separate spin probe dynamics and overall protein dynamics, to characterize protein backbone dynamics, and to resolve protein conformational states.

Keywords Multifrequency electron paramagnetic resonance (EPR) · Protein dynamics · Spin probe motion · Site-directed spin labeling

Introduction

Protein dynamics is crucial for biological function, especially for ATPases and regulatory proteins. Protein struc-

Y. E. Nesmelov (✉) · D. D. Thomas
Department of Physics and Optical Science,
University of North Carolina,
9201 University City Boulevard,
Charlotte, NC 28223, USA
e-mail: yuri.nesmelov@uncc.edu

tural change is usually a requirement for ATPase activity during the interaction with a nucleotide. Conformational sampling is a requirement for successful function of a regulatory protein. The combination of site-directed spin labeling (SDSL) and electron paramagnetic resonance (EPR) is a well-established method to determine protein dynamics and protein conformations (Berliner 1976). Following protein site-directed cysteine mutagenesis, a nitroxide spin probe covalently binds to the mutated Cys residue and reports on local dynamics of the probe itself, conformational dynamics of protein domains, and global protein tumbling. Anisotropy of the nitroxide spin probe magnetic tensors provides exceptional sensitivity and resolution of EPR to probe orientation in the external magnetic field, producing high-resolution sensitivity to the spin probe's rotational motion.

Several motional models have been developed to interpret EPR spectra of a spin probe in terms of its dynamics. Simple models, based on partial averaging of nitroxide magnetic tensors, are applicable to the approximation of fast (subnanosecond) and restricted motion of a spin probe, and are useful to describe protein conformation at the labeling site (Timofeev and Nikolsky 2003; Van et al. 1974). In this model, the EPR lineshape depends only on parameters describing the restriction of spin probe motion, e.g., the cone angle in a wobbling-in-cone model (Van et al. 1974) or the angle of oscillation (Timofeev and Nikolsky 2003). Advanced models, based on quantum mechanical description of evolution of spin probe ensemble magnetization, were developed to model slow restricted motion of a spin probe within a protein, and protein overall tumbling in solution (Freed 1976; Hustedt et al. 1997; Robinson et al. 1992). In this case, more parameters are required to describe the spin probe EPR lineshape: diffusion tensors that reflect the rotational rates and anisotropies of both spin

probe and protein, and potentials that reflect restrictions of these motions. These variable parameters, along with unknown spin–spin relaxation time of a probe (responsible for EPR spectra broadening), make fits of single-frequency EPR spectra ambiguous. For example, the effects of increased rotational rate can be hard to distinguish from those of increased rotational amplitude. This ambiguity is greatly decreased in a simultaneous fit of EPR spectra that are obtained for the same labeled protein at different frequencies. Ambiguity is reduced because of the sensitivities of EPR spectra to rotational rates and amplitudes are quite frequency dependent.

EPR and nitroxide: winning combination

Resolution to spin probe orientation in the external magnetic field

In the nitroxide radical, an unpaired electron is localized in the π orbital of the N–O bond, with the z-axis oriented perpendicular to the N–O bond, and the x-axis oriented parallel to the N–O bond (Fig. 1). This asymmetry of electron density leads to orientation dependence of the nitroxide EPR lineshape in the external magnetic field. The distribution of the unpaired electron density in the nitroxide is reflected in the g-factor tensor (Equation 1).

$$H = (h\nu)/(g\beta_e) + m_1 A, \tag{1}$$

where H is the resonant magnetic field, ν the resonant frequency, h Planck's constant, β_e Bohr's magneton, $m_1 = (-1, 0, +1)$ the nitrogen nuclear spin quantum number, and A the hyperfine splitting tensor. Equation 1 determines the magnetic field of resonance; the higher the EPR frequency, the better resolution for g-factor components (first term in Equation 1). The interaction of the unpaired electron with the nitrogen nucleus results in splitting of the EPR line into a triplet (due to the second term in Equation 1). The splitting is orientation-dependent and determined by the electron–nucleus hyperfine interaction tensor A. Higher electron density in the z direction produces larger electron–nucleus interaction and consequently a larger EPR line splitting when the z axis of the spin probe is oriented parallel to the external magnetic field. y- and x-components of electron density are smaller, producing smaller line splitting when y- or x-axes of the nitroxide are oriented along the magnetic field H. The value of the hyperfine splitting does not depend on the frequency ν (Equation 1), so the center of each triplet spectrum is determined entirely by the g-tensor and depends on frequency ν (first term in Equation 1). Increasing ν increases the resolution of the x-, y-, and z-components in the EPR spectrum. Thus, the resolution to g-factor spectral components becomes comparable to the hyperfine splitting A_z at 1.036 T, and 29.094 GHz for a typical nitroxide (g_x=2.0087, g_y=2.0058, g_z=2.0018, A_x=7.1 G, A_y=7.2 G, A_z=36.7 G). At lower magnetic field and frequency (for example, 0.34 T, 9.4 GHz, X-band), the lineshape of the nitroxide EPR spectrum is determined mainly by the anisotropy of the hyperfine tensor, while in higher fields (3.4 T, 94 GHz, W-band), both g-tensor and hyperfine tensor contribute to EPR spectral lineshape (Figs. 1 and 2).
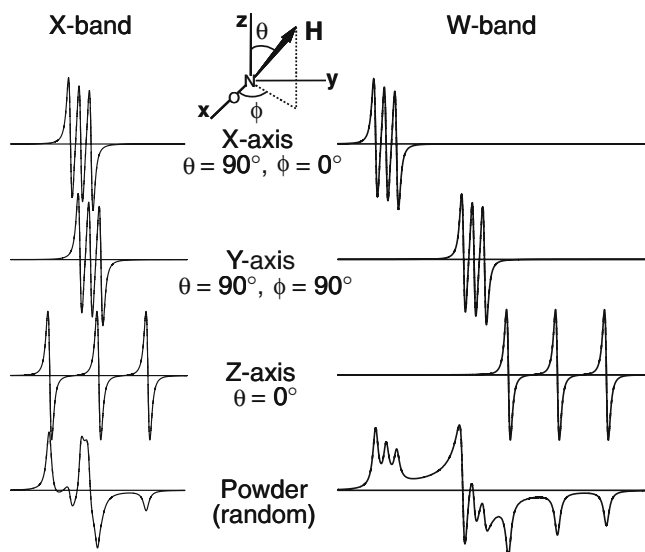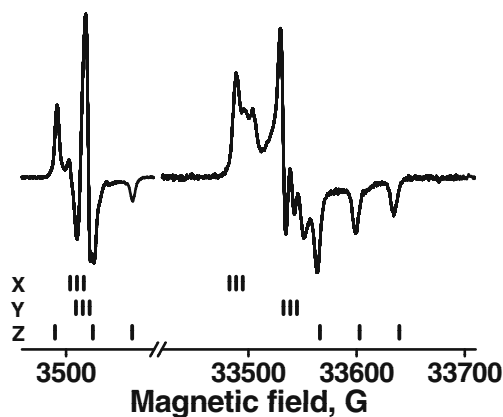

Fig. 1 The position and splitting of the nitroxide spin probe EPR spectrum depends on probe orientation in the external magnetic field H (Equation 1). In the "powder" spectrum all spin probes' orientations are present. Resonance line position and splitting depends on tensors g and A, respectively. H=0.34 T, ν=9.4 GHz (X-band), H=3.4 T, ν= 94 GHz (W-band)

Fig. 2 X-band (0.34 T, 9.4 GHz) and W-band (3.4 T, 94 GHz) "powder" EPR spectra of iodoacetamido-TEMPO-labeled myosin head S1. x, y, and z are the spectral components of g and A tensors, not resolved in X-band and clearly resolved in W-band due to better g-factor resolution

Resolution to spin probe dynamics

Fast isotropic motion averages g- and A-tensors of the nitroxide spin probe, reducing them to scalar values $g_0 = 1/3 (g_x + g_y + g_z)$, and $A_0 = 1/3(A_x + A_y + A_z)$ and producing a three-line EPR specrtrum, similar to the EPR spectrum of an oriented nitroxide in the absence of motion (Fig. 3, top left). The frequency of averaging motion for A- and g-tensors is, accordingly, $2\pi(A_z - A_x)\beta_e g_0/h$ and $2\pi(g_x - g_z)\beta_e H/h$. Rotational motion of a spin probe much faster than these averaging frequencies does not change the EPR spectrum lineshape, while slower significantly changes the EPR lineshape, until the powder limit is reached (Fig. 3, bottom row). The restrictions of a spin probe motion also affect the EPR lineshape (Fig. 3, left to right). Another factor affecting the EPR lineshape is the spin–spin relaxation time, T_2, of the nitroxide, which contributes to the linewidth.

EPR spectra interpretation and fit

There are several models to describe spin probe dynamics. The simplest model assumes fast motion of a spin probe much faster than the averaging rate. Restrictions of spin probe motion lead to partial averaging of the magnetic tensors and a more complex EPR spectrum lineshape. Several models of motion are developed to describe different character of a fast motion of a spin probe: wobbling in a cone, uniaxial rotation, or limited angle oscillations (Van et al. 1974; Nordio 1976; Timofeev and Nikolsky 2003). The spectral lineshape depends on the angle of oscillation (or the angle of a cone); the angle can be immediately found from the apparent hyperfine splitting, A_z', due to the relationship of A_z (the value of z-component of hyperfine splitting tensor, found for immobilized spin

probe) and A_z' (apparent value of z-component of hyperfine splitting tensor, determined from the spectrum) in Euler transformations (Van et al. 1974). High frequency and low frequency EPR spectra are equivalent in these models, the high frequency EPR experiment provides better insight into the character of a spin probe motion due to better resolution of x, y, and z spectral components.

A more complex model, assuming slow and restricted motion of a spin probe, considers the evolution of the total magnetization of the sample. Two approaches are developed currently, the microscopic order, macroscopic disorder (MOMD) approach, assuming slow and restricted motion of a spin probe within randomly distributed immobile protein molecules (Freed 1976). The slow relaxing local structure (SRLS) approach (Polimeno and Freed 1995) assumes slow restricted motion of a spin probe within a protein, which itself tumbles in solution. Slow motion of a spin probe is described with the diffusion coefficient D_R; usually, the diffusion coefficient of a spin probe has tensor value. To account for isotropic tumbling of labeled protein, additional diffusion coefficient is introduced. The restrictions of spin probe motion within the protein are modeled with irreducible spherical harmonic functions, using their coefficients as variable parameters in the EPR spectral fits (Budil et al. 1996). Figure 3 shows simulated X-band EPR spectra for a spin probe moving isotropically in a Maier-Saupe potential (Freed 1976), the first term of the spherical harmonics function series. According to Fig. 3, EPR spectra lineshape is extremely sensitive to spin probe motion on the nanosecond time scale, reflecting the spin probe's rotational correlation time and restrictions of motion, as well as resolving multiple populations of spin probes with different motions. Figure 3 also illustrates how hard it is to distinguish between spectra of spin probe with slow unrestricted motion and fast restricted motion; the outer extrema splittings are similar for these types of spin probe

Fig. 3 Lineshapes of nitroxide spin probe EPR spectra (X-band, *left panel*, and W-band, *right panel*, X- and W-band spectra are not to scale) at different rotational correlation times and order parameters (reflecting restriction of motion modeled as a Maier-Saupe potential; Freed 1976)
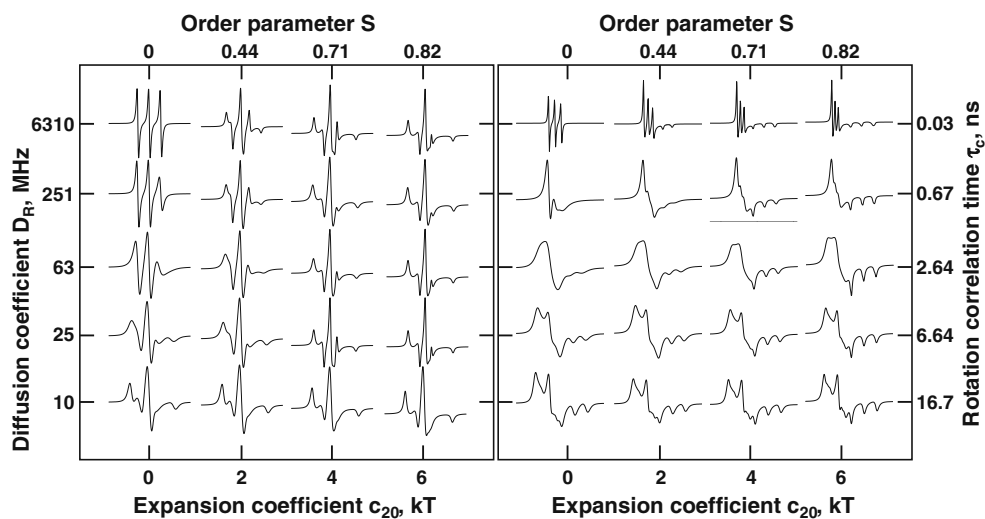
motion. The lines of EPR spectrum are narrower for a faster moving spin probe, but spectral broadening, usually unknown due to the unknown spin probe's relaxation time T_2, masks sharp spectral features, making it hard to distinguish the spectral response of a spin probe's fast restricted motion or slow unrestricted motion. This problem is solved in multifrequency EPR, which can distinguish between fast restricted and slow unrestricted spin probe motion.

Analysis of EPR spectra, obtained at different frequencies

Two tensors, g-factor and hyperfine splitting tensor A, determine the magnetic properties of a spin probe and the lineshape of its EPR spectrum (Equation 1). The g-tensor determines the value of resonant magnetic field; the resolution of x-, y-, and z-components of the g-tensor depends on the frequency of the resonance: the higher the microwave frequency, the better the resolution to g-tensor components (Fig. 2). The value of the hyperfine splitting does not depend on resonant frequency and remains constant. Molecular motion of a spin probe modulates both tensors, and the modulation of g- and A-tensors depends on the microwave frequency, making multifrequency EPR a valuable tool to determine the molecular dynamics of a spin probe, and the labeled protein.

To illustrate the difference in the effect of molecular motion on g- and A-tensors at different microwave frequencies, one can consider the motion that averages the tensors. The frequency of spin probe motion that averages the g-tensor can be calculated as $2\pi(g_x - g_z)\beta_e H/h$, which depends linearly on the resonant magnetic field strength H. The greater H, the higher is the averaging frequency of spin probe motion (Fig. 4, "g-factor averaged"). In contrast, the frequency of averaging for the A-tensor is $2\pi(A_z - A_x)\beta_e g_0/h$, independent of H (Fig. 4, "hyperfine splitting averaged"). The area under the lines "g-factor" and "hyperfine splitting" represents the spin probe motional regime with non-averaged tensors g and A; the area above these lines represents motion, averaging g- and A-tensor values, respectively. Thus, at X-band (9 GHz, 0.34 T), the g-tensor gets averaged at slower spin probe motion than the A-tensor. At W-band (94 GHz, 3.4 T), this is reversed (Fig. 4), so the W-band EPR spectrum is sensitive to faster motion. At a certain rate, both g- and A-tensors at X-band are completely averaged, but at W-band, the g-tensor is still anisotropic. This simple consideration of the rate of molecular motion, averaging tensors g and A, explains the different sensitivity of the EPR experiment at different frequency to a molecular motion.

Initially, the multifrequency approach for EPR spectral analysis was realized separately for higher and lower
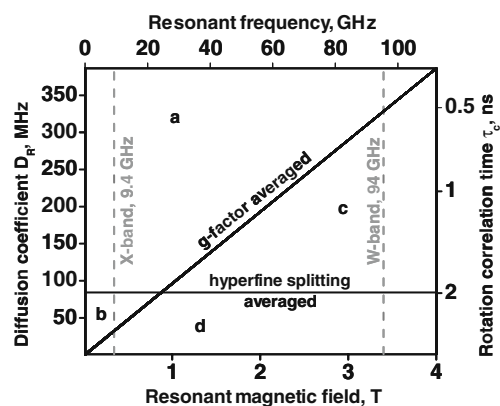

Fig. 4 The effect of molecular motion on g- and A-tensors averaging. Field position of g-components is frequency dependent and at higher resonant frequency g-factor averages at faster motion rate. The value of hyperfine splitting does not depend on resonant frequency and averaged A-tensor value is a constant number. **a** Both g- and A-tensors are averaged, three line EPR spectrum; **b** g-tensor is averaged, A-tensor is not; **c** g-tensor is not averaged, A-tensor is averaged; **d** both g- and A-tensors are not averaged

frequency EPR. First, the high-frequency EPR spectrum was fitted in the MOMD approach, assuming the absence of protein tumbling, to determine spin probe rotational dynamics (correlation times, order parameters). Then, the determined parameters of spin probe motion were fixed in the fit of low frequency EPR spectra to determine the diffusion coefficient of labeled protein global tumbling in solution (Barnes et al. 1999; Borbat et al. 2001). It was shown later that even at high frequency, global tumbling affects the EPR spectrum lineshape (Liang et al. 2004), and simultaneous fit of spectra at all frequencies was adopted with SRLS (Liang et al. 2004; Sezer et al. 2009).

The choice of "good" initial parameters for a spectral fit is important. The multifrequency approach decreases the ambiguity in this case. The analysis of EPR spectra splitting at different frequencies helps to narrow the region of the initial parameters, leading to convergence in multifrequency spectra fit (Nesmelov et al. 2007).

T4L-MTSSL dynamics in solution

Bacteriophage T4 lysozyme (T4L) is a well-characterized enzyme in terms of structure and stability, and was chosen as a model system to study protein backbone flexibility and side chain dynamics (Barnes et al. 1999; Borbat et al. 2001; Columbus and Hubbell 2002; Columbus et al. 2001; Liang et al. 2004; Sezer et al. 2009). Several residues of Cys-less T4L were mutated to cysteine and labeled with MTSSL: S44 and Q69 (Barnes et al. 1999; Borbat et al. 2001), D72 and V131 (Liang et al. 2004; Sezer et al. 2009). All mutated residues are solvent exposed and located on alpha helices. For S44C and Q69C, EPR spectra at 9 and 250 GHz were

acquired (T=10C) (Barnes et al. 1999; Borbat et al. 2001); for D72C and V131C, EPR spectra at 9, 94, 170, and 250 GHz were acquired at different temperatures (T=2°C–37.5°C) (Liang et al. 2004; Sezer et al. 2009). Multifrequency EPR spectra were fitted sequentially (high frequency first, to determine local motion of a spin probe in the MOMD approach, and then low frequency to determine global tumbling of labeled protein, in the SRLS approach) (Barnes et al. 1999; Borbat et al. 2001; Liang et al. 2004), or simultaneously in the SRLS approach (Liang et al. 2004). All studies were agreed on the diffusion coefficient for lysozyme global tumbling at T=10°C, τ_c=11–15 ns (Barnes et al. 1999; Liang et al. 2004). All four labeling sites showed a two-component EPR lineshape, especially at a lower temperature (Liang et al. 2004). The motion of a spin probe at all labeling sites was determined to be anisotropic for both populations; with sub-nanosecond correlation time about x and y axes and tens of nanoseconds correlation time in the x–y plane about the z axis ($\tau_\perp = 0.08ns - 0.8ns$, except for the minor population of V131C, $\tau_\perp = 6.4ns$, and for the minor population of Q69C, τ_y=2.1–3.3 ns; $\tau_\parallel = 3.7ns - 33ns$, except for the major population of Q69C, $\tau_\parallel = 0.4ns - 0.8ns$). The restoring potential for a spin probe is characterized by two coefficients, c_{20} and c_{22}; the motion of the major component is less restricted than the motion of the minor component (major component, c_{20}=0.8–2.8 kT, c_{22}=−1.7 to 0.6 kT; minor component, c_{20}=2.0–2.5 kT, c_{22}=−1.5 to −2.1 kT; except for S44C and Q69C, minor component, c_{20}=4.1 kT–5.2 kT). The mean distribution of spin label orientation for both components is shown in Fig. 5 (major component, c_{20}=1.8 kT, c_{22}=−0.5 kT; minor component c_{20}=3.8 kT, c_{22}=−1.8 kT).

The recently developed approach of EPR spectra simulation from MD trajectories gives a detailed look at the spin probe orientation and interaction with surrounding residues. Analysis of D72C and V131C labeling sites (Sezer et al. 2009) shows that spin probe indeed accepts two conformations, due to a large energy barrier for motion
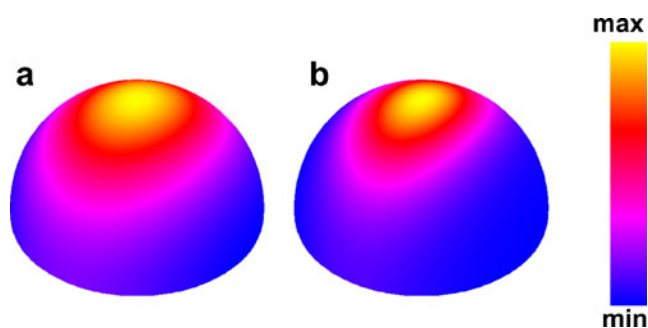

Fig. 5 MTSSL at T4 lysozyme: two populations of the spin probe within protein, with less (a) and more (b) restricted motion. Probability distributions of the probe's z-axis orientation, obtained from 9 and 250 GHz EPR spectra

around the disulfide bond. It was shown previously that alanine mutation of adjacent residues on the helix ($i\pm3$, $i\pm 4$) does not affect X-band EPR spectra of labeled T4L (Columbus and Hubbell 2002; Mchaourab et al. 1996). MD simulations show that the spin probe participates in diverse hydrophobic and electrostatic interactions with several neighbor residues simultaneously, which restricts the spin probe motion and explains the absence of dramatic effect of $i\pm3$, $i\pm4$ alanine mutations.

TOAC-PLB dynamics in a membrane

Phospholamban (PLB) is a 52-amino-acid amphipathic integral membrane protein that regulates the active transport of calcium in the heart through the interaction with the cardiac sarcoplasmic reticulum Ca-ATPase (SERCA) (MacLennan and Kranias 2003; Reddy et al. 1999). The NMR structure of monomeric PLB in detergent micelles (PDB 1N7L) (Zamoon et al. 2003) reveals a predominant L-shaped conformation with two approximately perpendicular helices, cytoplasmic (residues 1–16) and transmembrane (residues 21–52), connected by a flexible hinge. According to solid-state NMR (Mascioni et al. 2002; Traaseth et al. 2006) and EPR (Karim et al. 2004; Kirby et al. 2004), PLB's predominant conformation in the membrane has the transmembrane domain approximately perpendicular to the membrane. NMR data show the cytoplasmic domain oriented almost perpendicular to the transmembrane domain, lying along the membrane surface and interacting with lipid headgroups. EPR quenching studies confirm interaction of cytoplasmic domain with the surface of membrane (Karim et al. 2004). However, cross-linking (James et al. 1989) and functional mutagenesis (Toyofuku et al. 1994) data suggest that the cytoplasmic domain of PLB extends well above the membrane surface when it interacts with SERCA, so most models of the PLB-SERCA complex show PLB straightened almost linearly on the surface of SERCA, with the entire molecule, including the cytoplasmic domain, nearly perpendicular to the membrane surface (Hutter et al. 2002; Karim et al. 2004, 2006; Toyoshima et al. 2003; Zamoon et al. 2005).

To understand how PLB undergoes this dramatic structural transformation in a membrane, PLB labeled with TOAC (paramagnetic amino acid that reports directly the dynamics of the peptide backbone; Karim et al. 2004) was synthesized. TOAC-PLB was reconstituted into DOPC/DOPE lipid vesicles (1/200 protein/lipid ratio), EPR spectra were acquired at 9.4 and 94 GHz at T=4C. The spin probe was strongly immobilized, when TOAC is inserted into the transmembrane domain of PLB, consistent with a well-ordered α-helix. It was determined that the transmembrane domain rotates slowly ($\tau_\parallel = 105ns$) around the helix axis

and performs a rapid ($\tau_\perp = 2ns$), but very restricted ($c_{20}=14$ kT) wobbling motion perpendicular to this axis in the membrane (Fig. 6). TOAC-PLB with the labeled site in the cytoplasmic domain shows clear evidence for two resolved conformations, one a well-ordered helix (the T conformation, $\tau_{iso}=3.5$ ns, $c_{20}=4.2$ kT, 84% mole fraction; Fig. 6b), and the other dynamically disordered on the nanosecond time scale (the R conformation, $\tau_{iso}=0.68$ ns, $c_{20}=0.52$ kT, 16% mole fraction; Fig. 6c). The disordered R conformation binds preferentially to SERCA (Karim et al. 2006; Zamoon et al. 2005) and is enhanced by phosphorylation of PLB (Karim et al. 2006), resulting in SERCA activation. The T conformation interacts with the surface of the membrane, slowing its motion and stabilizing its helical conformation. It is likely that the large rate and amplitude of the cytoplasmic helix rotational motion is due, at least in part, to the partial unfolding of this helix, as suggested previously by both NMR (Metcalfe et al. 2004) and EPR (Karim et al. 2004) data.

Myosin S1-IASL dynamics in solution

Myosin is a motor enzyme involved in muscle contraction and cell motility through a cycle of actin-activated ATP hydrolysis. Myosin's head domain, subfragment 1 (S1), is responsible for the coupling of ATP hydrolysis and force generation. During the ATPase cycle, myosin shows two dramatic conformational changes, the powerstroke, when the force gets generated, and the recovery stroke, when myosin molecule primes to perform a powerstroke. Three structural states of myosin were originally identified by intrinsic fluorescence (Bagshaw and Trentham 1974; Johnson and Taylor 1978): M, the apo state, M*, the post-powerstroke state, trapped with ADP nucleotide, and M**, the pre-powerstroke state, trapped with ADP.Vi. These structural states are assumed to be tightly coupled to

biochemical states, which are defined by the nucleotide bound to the active site. These conformational states of myosin S1 have also been observed and characterized by EPR through the changes in mobility of a nitroxide spin probe (IASL) at the SH1 labeling site (C707) (Agafonov et al. 2008; Barnett and Thomas 1987; Nesmelov et al. 2008; Ostap et al. 1993; Seidel et al. 1970) in the force-generating region of myosin.

Magnetic tensor values were determined from fitting of W-band EPR spectra of IASL-S1 at T=80 K, and were kept constant. The rotational correlation time of global S1 tumbling were determined as $D_{Riso}=1.3\times10^6$ rad^2 s^{-1}, $\tau_c=128$ ns (Nesmelov et al. 2008) and was kept constant. The rotational correlation time and restrictions of spin label motion within myosin, Lorentzian broadening, and the angle between the magnetic frame and the diffusion frame of the spin label (β_d) were variable parameters. Figure 7 shows the probability of the spin label orientation distribution for each biochemical state of IASL-S1. In the apo S1 biochemical state, multifrequency EPR unambiguously detects a single structural state of myosin in the force-generating domain, M. The motion of the spin label is complex; the molecular frame of the spin label is tilted in the diffusion frame ($\beta_d=32°$), the spin probe moves slowly on the nanosecond time scale ($\tau_\perp = 9.9ns$, $\tau_\parallel = 64ns$), and the motion is very restricted ($c_{20}=4.36$ kT), Fig. 7a. These slow restricted motions probably reflect those of the secondary structural elements in close contact with the labeled site. Indeed, our modeling of the structure of *D. discoideum* myosin in the apo S1 state (1FMV; Bauer et al. 2000) shows that the spin probe is located between the converter and N-terminal domains of myosin (Fig. 8). The spin label is squeezed between myosin domains, but not buried under the surface, since g- and A-tensor values do not reflect changes in polarity for different myosin states. In the S1.ADP state, a single structural state (M*) is also determined. In this conformation of the force-generating
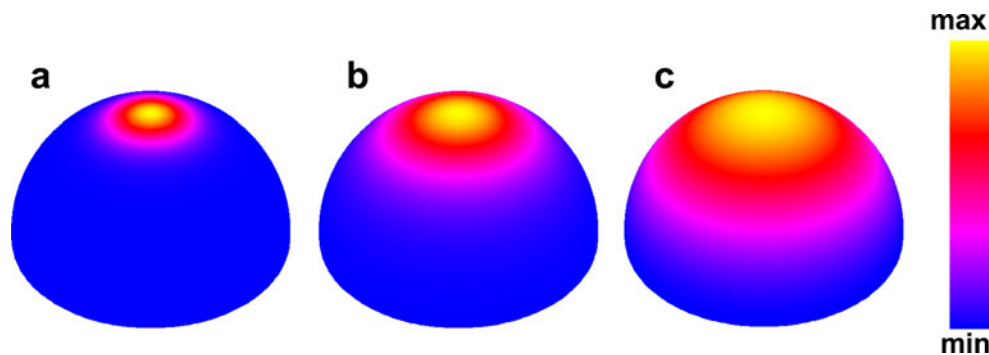

Fig. 6 TOAC-labeled PLB in lipid bilayer: probability distribution of PLB domains orientation in a membrane, revealed from 9.4 and 94 GHz EPR spectra. TOAC label is rigidly attached to PLB backbone and distribution of spin probe's z-axis orientation, measured by EPR reflects distribution of PLB domain orientations. **a** Transmembrane domain, very narrow distribution; **b** cytoplasmic domain, T conformation; **c** cytoplasmic domain, R conformation, practically unrestricted motion
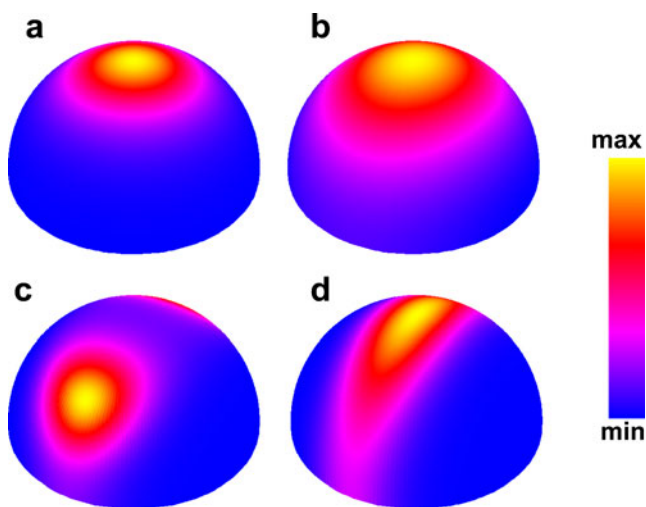
Fig. 7 IASL labeled myosin S1; the spin probe is located between the converter and N-terminal domains of myosin (Fig. 8). Orientational distribution of the spin probe's z-axis within myosin in three structural states, M, apo myosin (**a**), M*, myosin with ADP bound (**b**), M**, myosin with the nucleotide analog ADP.Vi bound (distributions (**c**) and (**d**)). Both distributions (**c**) and (**d**) reflect spin probe motion about its x axis, restricted (**c**) and unrestricted rotation (**d**). Domain flexibility on the microsecond time scale is proposed to explain two distributions of the spin probe orientation in one structural state of myosin (Agafonov et al. 2008; Nesmelov et al. 2008)

domain, the spin probe moves slightly faster, its motion is less restricted relative to the apo S1, and the tilt of the molecular frame of the spin label in the diffusion frame is less ($\tau_\perp = 6.8 ns$, $\tau_\parallel = 25.2 ns$, c_{20}=1.88 kT, c_{22}=−0.36 kT, β_d=5°), Fig. 7b. The structure of *D. discoideum* myosin with bound ADP (1MMA; Gulick et al. 1997) shows a slightly different position of the converter relative to N-terminal domain, compared to that of apo S1, allowing more space for the spin label to move, in qualitatively agreement with EPR data. A much more complex structural picture emerges in the S1.ADP.V_i complex, which is presumed to correspond to the pre-powerstroke structural state M**. The EPR spectrum in this complex shows at least two, and probably three, structural states, while only one structural state is revealed by the crystal structure, 1VOM (Smith and Rayment 1996). One spectral component (component 1, 16%) is similar to that of IASL-S1. ADP, suggesting the presence of M* structural state. The two other spectral components (corresponding to higher mobility, with mole fractions 78% and 6%) have different dynamics of the spin probe (component 2, 78%, τ_x=1.0 ns, τ_y=1.8 ns, τ_z>300 ns, c_{20}=4.96 kT, c_{22}=−4.91 kT, c_{40}=−1.93 kT; Fig. 7c; component 3, 6%, τ_x=0.2 ns, τ_y= 0.1 ns, τ_z>300 ns, c_{20}=6.42 kT, c_{22}=−6.24 kT; Fig. 7d), there is no tilt of the molecular frame relative to the diffusion frame. These spectral components could be assigned as the M** structural state of myosin (Barnett and Thomas 1987). According to the structure of the S1.ADP.

V_i state, the spin probe is located between the converter and N-terminal domains, while the relay helix is bent in this structural state and is not likely to affect spin label motion. The two observed distributions of spin label orientation in the M** structural state (78% and 6%) could reflect a slight difference in relative position of the converter and N-terminal domains: rotation of the spin label about the x axis is allowed in one state (M_1**, 6%; Fig. 7d) and stopped in another state (M_2**,78% Fig. 7c). This slight difference in relative position of domains within one myosin population (M**) could be interpreted in terms of flexibility between myosin domains in the M** state on the microsecond and slower time scale (Houdusse and Sweeney 2001), and could be treated as a slow exchange between myosin conformations, producing two spectral components.

Conclusion

Multifrequency EPR is a unique spectroscopic tool, allowing detailed characterization of protein dynamics. With multifrequency EPR, the spin probe's local dynamics can be unambiguously separated from protein overall tumbling. Analysis of spin probe motion within a protein reveals dynamics of protein domains and characterizes protein conformation. Multiple conformations of a spin labeled protein can be distinguished with multifrequency EPR. A model system, spin labeled T4 lysozyme, demonstrates these important features of the multifrequency EPR
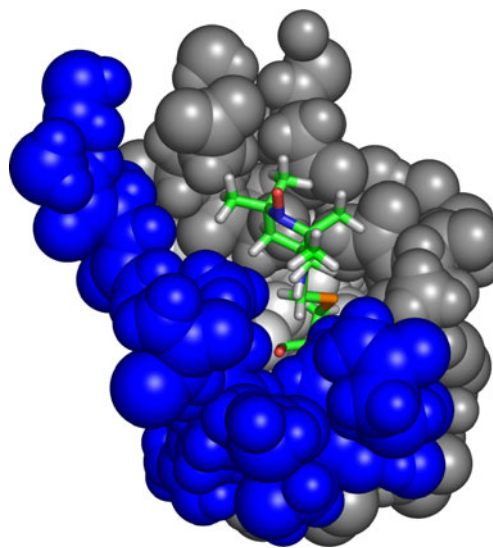

Fig. 8 IASL probe within myosin S1, squeezed between the converter domain (*blue*) and the N-terminal domain (*gray*). Pre-powerstroke M** structural state (1vom.pdb). According to Fig. 7c, d, the spin probe oscillates (c) or freely rotates (d) about its x-axis (N–O bond, *blue* and *red* atoms of the spin probe sticks image). Two spin probe distributions within one structural state M** might reflect domains flexibility within myosin on microsecond time scale

approach. Subsequent studies of TOAC-labeled phospholamban in lipid bilayer and IASL-labeled myosin in solution have used this approach for detailed characterization of functional dynamics of regulatory peptide in a membrane and structural changes of myosin during its conformational changes in the ATPase cycle. These studies confirm the unique properties of multifrequency EPR in determination of protein functional dynamics.

References

Agafonov RV, Nesmelov YE, Titus MA, Thomas DD (2008) Muscle and nonmuscle myosins probed by a spin label at equivalent sites in the force-generating domain. Proc Natl Acad Sci USA 105:13397–13402

Bagshaw CR, Trentham DR (1974) The characterization of myosin-product complexes and of product-release steps during the magnesium ion-dependent adenosine triphosphatase reaction. Biochem J 141:331–349

Barnes JP, Liang Z, Mchaourab HS, Freed JH, Hubbell WL (1999) A multifrequency electron spin resonance study of T4 lysozyme dynamics. Biophys J 76:3298–3306

Barnett VA, Thomas DD (1987) Resolution of conformational states of spin-labeled myosin during steady-state ATP hydrolysis. Biochemistry 26:314–323

Bauer CB, Holden HM, Thoden JB, Smith R, Rayment I (2000) X-ray structures of the apo and MgATP-bound states of Dictyostelium discoideum myosin motor domain. J Biol Chem 275:38494–38499

Berliner LJ (ed) (1976) Spin labeling theory and applications. Academic, New York

Borbat PP, Costa-Filho AJ, Earle KA, Moscicki JK, Freed JH (2001) Electron spin resonance in studies of membranes and proteins. Science 291:266–269

Budil D, Lee S, Saxena S, Freed J (1996) Nonlinear-least-squares analysis of slow-motion EPR spectra in one and two dimensions using a modified Levenberg-Marquardt algorithm. J Magn Reson A120:155–189

Columbus L, Hubbell WL (2002) A new spin on protein dynamics. Trends Biochem Sci 27:288–295

Columbus L, Kalai T, Jeko J, Hideg K, Hubbell WL (2001) Molecular motion of spin labeled side chains in alpha-helices: analysis by variation of side chain structure. Biochemistry 40:3828–3846

Freed JH (1976) Theory of slow tumbling ESR spectra for nitroxides. In: Berliner LJ (ed) Spin labeling: theory and applications. Academic, pp 53–132

Gulick AM, Bauer CB, Thoden JB, Rayment I (1997) X-ray structures of the MgADP, MgATPgammaS, and MgAMPPNP complexes of the *Dictyostelium discoideum* myosin motor domain. Biochemistry 36:11619–11628

Houdusse A, Sweeney HL (2001) Myosin motors: missing structures and hidden springs. Curr Opin Struct Biol 11:182–194

Hustedt EJ, Smirnov AI, Laub CF, Cobb CE, Beth AH (1997) Molecular distances from dipolar coupled spin-labels: the global analysis of multifrequency continuous wave electron paramagnetic resonance data. Biophys J 72:1861–1877

Hutter MC, Krebs J, Meiler J, Griesinger C, Carafoli E, Helms V (2002) A structural model of the complex formed by phospholamban and the calcium pump of sarcoplasmic reticulum obtained by molecular mechanics. Chembiochem 3:1200–1208

James P, Inui M, Tada M, Chiesi M, Carafoli E (1989) Nature and site of phospholamban regulation of the Ca2+ pump of sarcoplasmic reticulum. Nature 342:90–92

Johnson KA, Taylor EW (1978) Intermediate states of subfragment 1 and actosubfragment 1 ATPase: reevaluation of the mechanism. Biochemistry 17:3432–3442

Karim CB, Kirby TL, Zhang Z, Nesmelov Y, Thomas DD (2004) Phospholamban structural dynamics in lipid bilayers probed by a spin label rigidly coupled to the peptide backbone. Proc Natl Acad Sci USA 101:14437–14442

Karim CB, Zhang Z, Howard EC, Torgersen KD, Thomas DD (2006) Phosphorylation-dependent conformational switch in spin-labeled phospholamban bound to SERCA. J Mol Biol 358:1032–1040

Kirby TL, Karim CB, Thomas DD (2004) Electron paramagnetic resonance reveals a large-scale conformational change in the cytoplasmic domain of phospholamban upon binding to the sarcoplasmic reticulum Ca-ATPase. Biochemistry 43:5842–5852

Liang Z, Lou Y, Freed JH, Columbus L, Hubbell WL (2004) A multifrequency electron spin resonance study of T4 lysozyme dynamics using the slowly relaxing local structure model. J Phys Chem B 108:17649–17659

MacLennan DH, Kranias EG (2003) Phospholamban: a crucial regulator of cardiac contractility. Nat Rev Mol Cell Biol 4:566–577

Mascioni A, Karim C, Zamoon J, Thomas DD, Veglia G (2002) Solid-state NMR and rigid body molecular dynamics to determine domain orientations of monomeric phospholamban. J Am Chem Soc 124:9392–9393

Mchaourab HS, Lietzow MA, Hideg K, Hubbell WL (1996) Motion of spin-labeled side chains in T4 lysozyme. Correlation with protein structure and dynamics. Biochemistry 35:7692–7704

Metcalfe EE, Zamoon J, Thomas DD, Veglia G (2004) (1)H/(15)N heteronuclear NMR spectroscopy shows four dynamic domains for phospholamban reconstituted in dodecylphosphocholine micelles. Biophys J 87:1205–1214

Nesmelov YE, Karim CB, Song L, Fajer PG, Thomas DD (2007) Rotational dynamics of phospholamban determined by multifrequency electron paramagnetic resonance. Biophys J 93:2805–2812

Nesmelov YE, Agafonov RV, Burr AR, Weber RT, Thomas DD (2008) Structure and dynamics of the force-generating domain of myosin probed by multifrequency electron paramagnetic resonance. Biophys J 95:247–256

Nordio PL (1976) General magnetic resonance theory. In: Berliner LJ (ed) Spin labeling. Theory and application. Academic, New York, pp 5–52

Ostap EM, White HD, Thomas DD (1993) Transient detection of spin-labeled myosin subfragment 1 conformational states during ATP hydrolysis. Biochemistry 32:6712–6720

Polimeno A, Freed JH (1995) Slow motional ESR in complex fluids: the slowly relaxing local structure model of solvent cage effects. J Phys Chem 99:10995–11006

Reddy LG, Jones LR, Thomas DD (1999) Depolymerization of phospholamban in the presence of calcium pump: a fluorescence energy transfer study. Biochemistry 38:3954–3962

Robinson BH, Slutsky LJ, Auteri FP (1992) Direct simulation of continuous wave electron paramagnetic resonance spectra from Brownian dynamics trajectories. J Chem Phys 96:2609–2616

Seidel J, Chopek M, Gergely J (1970) Effect of nucleotides and pyrophosphate on spin labels bound to S1 thiol groups of myosin. Biochemistry 9:3265–3272

Sezer D, Freed JH, Roux B (2009) Multifrequency electron spin resonance spectra of a spin-labeled protein calculated from molecular dynamics simulations. J Am Chem Soc 131:2597–2605

Smith CA, Rayment I (1996) X-ray structure of the magnesium(II). ADP.vanadate complex of the *Dictyostelium discoideum* myosin motor domain to 1.9 A resolution. Biochemistry 35:5404–5417

Timofeev VP, Nikolsky DO (2003) The role of the fast motion of the spin label in the interpretation of EPR spectra for spin-labeled macromolecules. J Biomol Struct Dyn 21:367–378

Toyofuku T, Kurzydlowski K, Tada M, MacLennan DH (1994) Amino acids Lys-Asp-Asp-Lys-Pro-Val402 in the Ca(2+)-ATPase of cardiac sarcoplasmic reticulum are critical for functional association with phospholamban. J Biol Chem 269:22929–22932

Toyoshima C, Asahi M, Sugita Y, Khanna R, Tsuda T, MacLennan DH (2003) Modeling of the inhibitory interaction of phospholamban with the Ca2+ ATPase. Proc Natl Acad Sci USA 100:467–472

Traaseth NJ, Buffy JJ, Zamoon J, Veglia G (2006) Structural dynamics and topology of phospholamban in oriented lipid bilayers using multidimensional solid-state NMR. Biochemistry 45:13827–13834

Van SP, Birrell GB, Griffith OH (1974) Rapid anisotropic motion of spin labels. Models for motion averaging of the ESR parameters. J Magn Res 15:444–459

Zamoon J, Mascioni A, Thomas DD, Veglia G (2003) NMR solution structure and topological orientation of monomeric phospholamban in dodecylphosphocholine micelles. Biophys J 85:2589–2598

Zamoon J, Nitu F, Karim C, Thomas DD, Veglia G (2005) Mapping the interaction surface of a membrane protein: unveiling the conformational switch of phospholamban in calcium pump regulation. Proc Natl Acad Sci USA 102:4747–4752